arXiv:1701.00022v3 [cond-mat.supr-con] 12 Jan 2017

# Precursor Charge Density Waves in $La_{1.875}Ba_{0.125}CuO_4$

H. Miao,[1,*] J. Lorenzana,[2] G. Seibold,[3] Y.Y. Peng,[4] A. Amorese,[5] F. Yakhou-Harris,[5] K. Kummer,[5] N. B. Brookes,[5] R. M. Konik,[1] V. Thampy,[1] G. D. Gu,[1] G. Ghiringhelli,[4] L. Braicovich,[4] and M. P. M. Dean[1,†]

[1] *Condensed Matter Physics and Materials Science Department, Brookhaven National Laboratory, Upton, New York 11973, USA*
[2] *ISC-CNR, Dipartimento di Fisica, Università di Roma "La Sapienza", P. Aldo Moro 2, 00185 Roma, Italy*
[3] *Institut für Physik, BTU Cottbus, P.O. Box 101344, 03013 Cottbus, Germany*
[4] *CNR/SPIN, CNISM and Dipartimento di Fisica, Politecnico di Milano, piazza Leonardo da Vinci 32, 20133 Milano, Italy*
[5] *European Synchrotron Radiation Facility (ESRF), BP 220, F-38043 Grenoble Cedex, France*

(Dated: January 16, 2017)

The observation of charge density wave (CDW) correlations in numerous different samples has provided increasing support to the concept that these correlations are an intrinsic property of the high temperature superconducting cuprates. It has long been hypothesized that long-range CDW order arises from the pinning of precursor high-temperature CDW fluctuations, but while precursor spin density wave (SDW) correlations have been studied in detail, the corresponding transition between long-range ordered and precursor CDW correlations has never been observed. Here we report the discovery of precursor CDW correlations in $La_{1.875}Ba_{0.125}CuO_4$. The precursor CDW has a correlation length of a few unit cells and exists at a different wavevector from the low temperature CDW decoupled from the SDW correlations. We find that the CDW and SDW correlations lock together at low temperature to form a phase with meandering partially ordered CDW correlations, reconciling the apparently different properties of the charge correlations in different cuprates.

When holes are doped into the Mott insulating parent compounds of the cuprates, multiple competing interactions conspire to form a rich phase diagram. In the underdoped regime, holes can save energy by clustering together on neighboring sites in order to minimize the number of broken magnetic bonds, but by doing so they pay an extra energy cost of the increased Coulomb repulsion. Several early theoretical works suggested that frustration between these different ordering tendencies generates an instability towards charge and spin density wave order [1–3]. Such concepts were key to the discovery of CDW order, often referred to as stripes, in the $La_{2-x-y}Nd_y(Sr/Ba)_xCuO_4$ or "214" family of cuprates [4, 5], in which it was hypothesized that tilting of the copper-oxygen octahedra in the low temperature tetragonal (LTT) crystal structure acted to pin dynamic precursor CDW correlations into a static CDW. However, directly detecting such precursor correlations proved beyond the sensitivity of standard x-ray and neutron scattering measurements. Many years after this initial discovery, the idea of a universal tendency towards CDW order was bolstered by the observation of CDW correlations in various other cuprate systems such as $YBa_2Cu_3O_{6+x}$ (YBCO), $Bi_{1.5}Pb_{0.5}Sr_{1.54}CaCu_2O_{8+\delta}$ (BSCCO2212), and $HgBa_2CuO_{4+\delta}$ (HBCO1201) [6–13]. Many of the CDW properties reported in these materials were, however, notably different than that in $La_{1.875}Ba_{0.125}CuO_4$ in terms of correlation lengths, ordering wavevectors and the relationship between the charge and spin correlations. On this basis, concepts such as nesting and electron-phonon coupling for CDW formation in YBCO, BSCCO, and HBCO were discussed extensively impeding efforts to understand these cuprates using similar mechanism that were discussed for "214" systems [9, 14–17]. Here we use new RIXS instrumentation to discover weak precursor CDW correlations in the high temperature phase of the canonical stripe-ordered cuprate $La_{1.875}Ba_{0.125}CuO_4$ [5, 18–20], with a different wavevector and unlocking between the charge and spin degree of freedom, reconciling the apparently different properties of the correlations in different cuprates.

## RESULTS

Figure 1a show the angles and scattering geometry employed here. By using Cu $L_3$ edge RIXS we exploit the resonant process to increase our sensitivity to the valence electrons while rejecting the fluorescence background that limits the sensitivity of standard soft x-ray resonant scattering experiments, achieving extremely high sensitivity. We further exploit the RIXS cross-section to examine both charge and spin scattering (see Supplementary Fig. 1) [6, 21, 22]. Figure 1b depicts the locations of the charge and spin ordering Bragg peaks for "214" type cuprates within the two-dimensional Brillouin zone labeled $\boldsymbol{Q}_{\rm CDW} \approx (0.24, 0)$ and $\boldsymbol{Q}_{\rm SDW} \approx (0.38, 0.5)$ in reciprocal lattice units (r.l.u.). We start by choosing $\sigma$ polarized incident x-rays in order to enhance our sensitivity to charge scattering [6, 21, 22]. Figure 1c,d plots projections of the quasi-elastic scattering intensity around $\boldsymbol{Q}_{\rm CDW}$ along the $H$ and the $K$ directions. A clear peak is observed at base temperature corresponding to the known CDW with a wavevector of $(0.235, 0)$ and a correlation length of 207(5) Å [18, 20]. As established in several previous studies the low temperature CDW peak

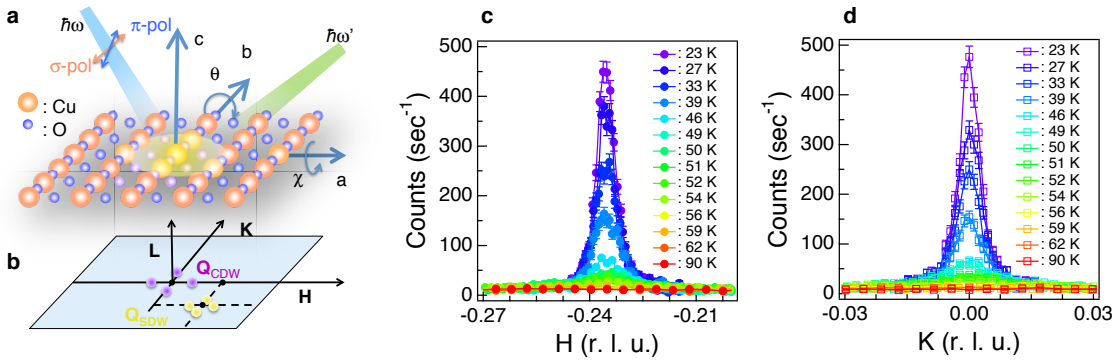


Figure 1. **Scattering geometry and temperature-dependent CDW Bragg peak. a**, The experimental geometry showing incident and outgoing photon directions, labeled by their energies of $\hbar\omega$ and $\hbar\omega'$, scattering from the $c$-axis face of the crystal. The incident x-ray polarization can be tuned to be parallel ($\pi$) or perpendicular ($\sigma$) to the scattering plane. **b**, The two dimensional (2D) cuprate Brillouin zone. Purple (yellow) points in the 2D Brillouin zone correspond to the locations of charge (spin) density wave Bragg peaks $\boldsymbol{Q}_{\rm CDW}$ and $\boldsymbol{Q}_{\rm SDW}$, respectively. **c** and **d** plot quasi-elastic RIXS intensity along $H$ and $K$, respectively, as a function of temperature, showing the CDW Bragg peak. Error bars in **c** and **d** represent the error from Poisson statistics.

intensity drops with increasing temperature and seems to disappear around 55 K [18, 20].

Having established the low temperature CDW properties, we scanned large regions of reciprocal space at temperatures above the nominal transition. Figure 2a-f plots RIXS intensity maps that reveal broad momentum-dependent scattering. The quasi-elastic intensity in these maps peaks around $(H, K) = (0.24, 0)$ for temperatures of 54-59 K, while at higher temperatures it peaks at larger $H$ while remaining centered at $K = 0$. Although the close match in the wavevectors between the low temperature and high temperature scattering already indicates an intimate connection between this scattering and the low temperature CDW, it is important to justify the electronic origin of the broad peak. Panels 2c (inset) and 2g show the off-resonance RIXS intensity map and integrated RIXS intensity along $H$. Both the inelastic excitations and the quasi-elastic remnant intensity are significantly suppressed when changing the incident energy, proving that the signal is dominated by the resonant process. The flat 2.8(0.3) counts sec$^{-1}$ off resonant intensity also confirms the constant spectrometer acceptance. We also see in Fig. 2i that the peak has the same width in $H$ and $K$, consistent with the behavior of the low temperature CDW (Fig. 1c,d). It is also worth noting that x-ray self-absorption effects (see Supplementary Fig. 2) and the Cu $L_3$ RIXS cross section are known to vary monotonically in this scattering geometry [6, 21]. Based on all these experimental observations, we conclude that the observed broad peak arises from CDW like-correlations and represents a direct observation of the precursor CDW correlations discussed extensively ever since the discovery of the low temperature CDW [4, 23–26]. Compared to the low-temperature CDW, the precursor CDW has far lower peak intensity (13 vs 467 counts/s) but a much broader line width (about a factor of 16). As a result, this diffuse precursor scattering comprises approximately 7 times larger 2D-momentum and energy integrated spectral weight than the low temperature CDW peak. No changes are observed in the diffuse precursor intensity, upon cooling through the transition. However, due to the relatively small amount of spectral weight in the CDW peak, the expected size of the change is likely to be below our signal-to-noise ratio.

The precursor CDW is often argued to be dynamic and such a view is supported by transport measurements [23, 24, 27]. Notably, long range ordered static LTT octahedral tilts, often thought to be coupled to the CDW at low temperatures, are found to become dynamic and correlated over a $\sim$ 10 Å lengthscale above the transition [28, 29]. On the basis of the resolution-limited energy width we observe (see Supplementary Fig. 4), we conclude that the precursor CDW is static on a timescale of $\sim$100 fs, but slow fluctuations are nonetheless possible and can, in principle be directly measured by other techniques [19]. This also relates to the interesting issue of how precursor CDW correlations couple to disorder [10, 30, 31].

Figure 3 shows the temperature dependence of the CDW correlations as determined by fitting Lorentzian-squared functions to the relatively sharp low temperature CDW peak and the much broader precursor peak intensity (see Supplementary Fig. 5 and Fig. 6). The correlation length of the precursor CDW of 13(2) Å is much shorter than that in the low temperature state (207 Å) and substantially shorter than YBCO (60 Å) [6], but is of the same order of magnitude to several other cuprates systems such as $Bi_2Sr_{2-x}La_xCuO_{6+\delta}$ (BSLCO2201) (12 Å) [9], BSCCO2212 (<24 Å) [12], $La_{2-x}Sr_xCuO_4$ (LSCO) (35 Å) [11], HBCO1201 (20 Å)

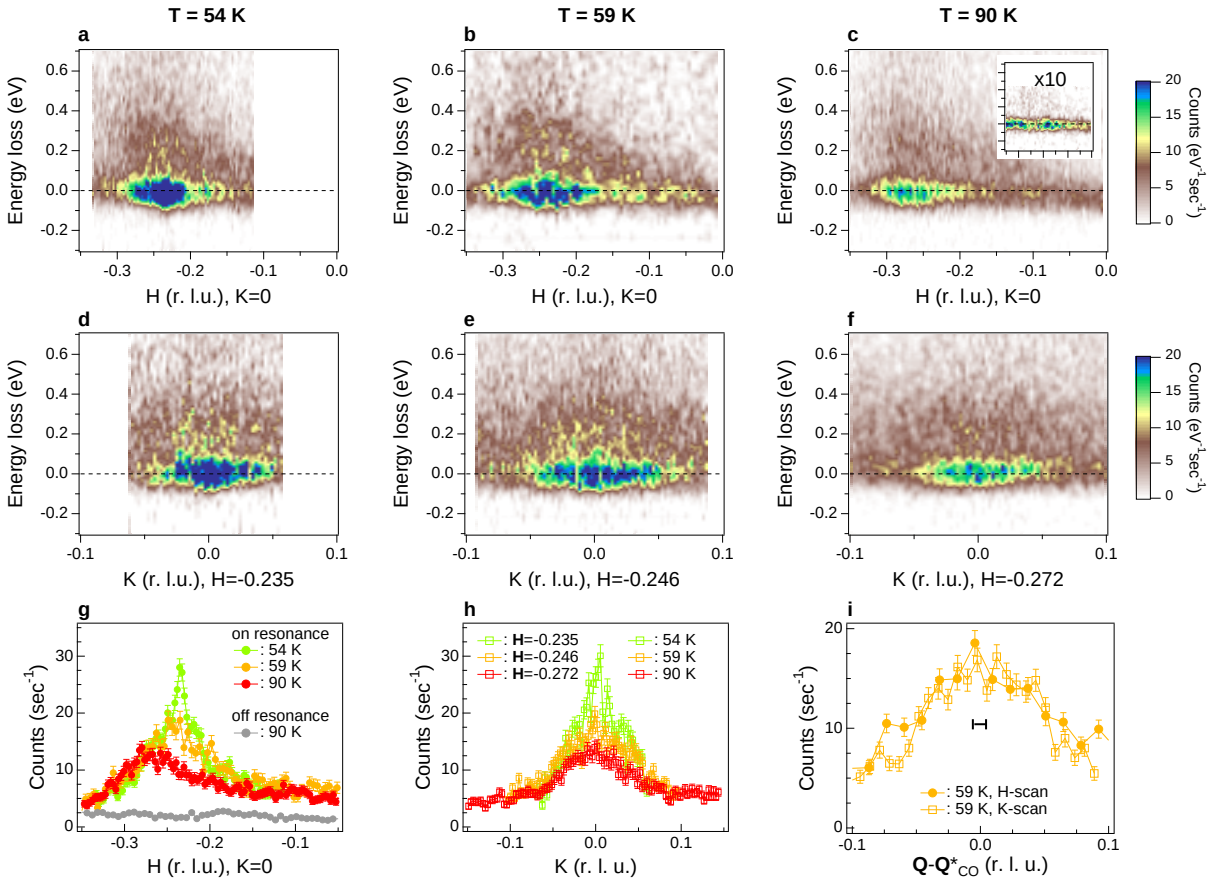


Figure 2. **Identification of the precursor-CDW**. **a-f** RIXS intensity at 54, 59 and 90 K cutting through the observed peak in the quasi-elastic intensity as a function of $H$ (**a-c**) and $K$ (**d-f**). A peak in the quasi-elastic intensity is seen in the vicinity of $\boldsymbol{Q}_{\rm CDW}$ alongside an increase in the inelastic intensity. The inset of panel **c** is the off-resonance intensity map at 90 K, which was multiplied by a factor of 10 to make the signal visible. **g**,**h** The quasi-elastic intensity calculated by integrating (**a-f**) confirming the presence of the peak. **i** Comparison of scans in the $H$ and $K$ directions showing similar widths parallel and transverse to the CDW similar to the low temperature behavior (Fig. 1 **c**,**d**). As discussed in the text, this scattering demonstrates the presence of precursor CDW correlations. Error bars in **g-i** come from Poisson counting statistics.

[13], hinting that the precursor CDW maybe help reconcile the difference between different cuprates.

A marked difference between the "214" family cuprates and other systems such as YBCO, BSCCO and HBCO is the apparent changes in the relationship between the CDW and SDW. As can be seen for temperatures below 55 K in Fig. 3b, the incommensurability of the CDW and SDW appear to be related by a factor of two. Indeed, $La_{2-x}Ba_xCuO_4$ has been shown to follow the so called "Yamada-plot" relation of $\boldsymbol{Q}_{\rm CDW} = 2\delta_{\rm SDW}$, where $\boldsymbol{Q}_{\rm SDW} = (0.5 - \delta_{\rm SDW}, 0.5)$ [5, 32–34] . Upon heating above 55 K, we see strong violation of this rule [Fig. 3b]: The CDW correlations evolve away from $H \approx 1/4$ and away from twice the incommensurability of the SDW (i.e. the CDW and SDW decouple). This strengthens the analogy to the low temperature CDW correlations in YBCO, BSCCO and HBCO. Indeed the $\boldsymbol{Q}_{\rm CDW} = 0.272(2)$ comes closer to what is seen in 1/8 doped YBCO and BSCCO2201, which are 0.32 and 0.27, respectively [6, 9]. In these materials the CDW and SDW wavevectors are also decoupled [6, 9] (in this case the SDW fluctuations are gapped [35]) and upon doping the evolution of $\boldsymbol{Q}_{\rm CDW}$ is opposite to the "Yamada-plot". It will be very important for future studies to measure whether the precursor CDW correlations in $La_{2-x}Ba_xCuO_4$ increase or decrease with $x$.

We further tested the nature of the CDW/SDW state and its charge-spin coupling by changing the RIXS geometry in order to measure the magnetic excitation spectrum in the same $\boldsymbol{Q}$-range (see Supplementary Fig. 1) [21]. Inelastic neutron scattering has been applied extensively to study the magnetic excitations around $\boldsymbol{Q}_{\rm SDW}$, finding an 'hour-glass' shaped dispersion [24, 36, 37], RIXS can study the magnetic spectrum around $\boldsymbol{Q}_{\rm CDW}$, a region of reciprocal space in which stripe-related effects have never been observed. Figure 4a-b shows the resulting spectral intensity above that is dominated by damped spin wave excitations called paramagnons [38–41]. The

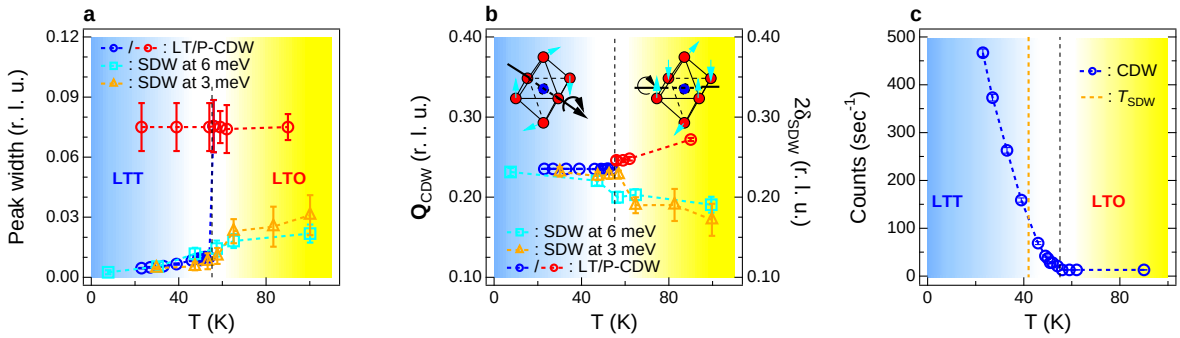


Figure 3. **Decoupling of the CDW and SDW in the precursor phase. a-c** The results of fitting the quasi-elastic intensity showing: **a** the full width at half maximum, **b** the incommensurability and **c** the intensity at the peak. The black dashed line at 54 K corresponds to the low temperature LTT-LTO structural phase transition which is depicted in **b**, blue and yellow code temperatures below and above this threshold [18]. The orange dashed line at 42 K in **c** represents the static SDW transition. The behavior of the SDW, taken from inelastic neutron scattering results at 3 and 6 meV energy transfer from Ref. [5] are included on panels **a** and **b**. We see that the CDW and SDW incommensurabilities evolve in different directions above 54 K, which indicates a decoupling of the charge and spin degrees of freedom. We also note that the precursor CDW (P-CDW) width and intensity show no detectable changes through the LTT-LTO transition (any possible changes would be smaller than our error bars, which are obtained from the least-squares fitting algorithm).

peak energies obtained by fitting the paramagnon lineshape are compared to the dispersion expected for a standard Néel antiferromagnet (AF) in Fig. 4c, finding a softening of the excitation energy over a broad range of reciprocal space around $\boldsymbol{Q}_{\rm CDW}$ (see Supplementary Fig. 7). The significant deviation observed at low temperatures shows that stripe-formation modifies the short-range spin correlations around $\boldsymbol{Q}_{\rm CDW}$ at low temperature, but this coupling is much reduced at higher temperatures, consistent with a weakened charge-spin coupling above the transition. There have been extensive efforts to model such stripe-related modifications in the spin excitation spectrum as this provides a means to develop detailed models for the character of the ground state [24, 37, 42–47]. These theories do a good job of capturing the magnetic dispersion around $\boldsymbol{Q}_{\rm SDW}$, but none of these theories adequately capture the dispersion around $\boldsymbol{Q}_{\rm CDW}$. We discovered that a partially ordered CDW state with meandering charge stripes (see the inset of Fig. 4d), as constrained by the measured charge scattering, does successfully capture the observed modification in the magnetic dispersion. Figure 4d plots our calculations (see the methods section for full details). Despite the simplicity of the model, it captures what is observed in Figure 4c, confirming that we have identified the essential features of the ground state. Calculations based on a perfectly stripe-ordered crystalline CDW predict several sharp modes which are not observed (see Supplementary Fig. 8).

## DISCUSSION

The different wavevectors and presence or absence of spin/charge locking has motivated discussion of a possible role for nesting and electron-phonon coupling mechanisms controlling CDW formation in YBCO and BSCCO [9, 14–17]. In $La_{1.875}Ba_{0.125}CuO_4$, which we study here, the evolution of the CDW wavevector shown in Fig. 3b puts strong constraints on the microscopic mechanism of CDW formation. Although the low temperature CDW wavevector is close to the vector that connects the endpoints of Fermi-arcs [48], its temperature evolution is opposite to that expected from simple nesting scenarios [9], where the expanded Fermi-arc would imply that the CDW wavevector should decrease at higher temperatures, opposite to what is observed here. We instead suggest that CDW formation mechanism based on the competition between superexchange, kinetic energy, and Coulomb interactions are more appropriate [1–3, 23, 24, 46]. The properties of the precursor CDW in $La_{1.875}Ba_{0.125}CuO_4$, is also very similar to that observed in YBCO and BSCCO pointing towards a universal picture for CDWs in all cuprates. These models usually assume a regular crystal of defects of the AF order which fails to describe correctly the magnetic excitation spectrum close to $\boldsymbol{Q}_{\rm CDW}$. We expect that meandering effects, that we find play an important role in explaining the magnetic excitation spectrum, would be need to be incorporated to describe the phenomenology of CDW in other compounds. For example, changes in wavevector can relate to changes in the meandering defects in the charge order [25, 26, 49].

From our observations, we can construct a detailed picture of CDW formation in $La_{1.875}Ba_{0.125}CuO_4$. Above

the nominal CDW transition temperature, the charge and spin degrees of freedom in $La_{1.875}Ba_{0.125}CuO_4$ are unlocked and the precursor CDW and SDW fluctuations exist at unrelated wavevectors. This precursor CDW state appears to be a universal property of the $CuO_2$ planes common to all superconducting cuprates. At low temperatures, however, this tendency towards different CDW and SDW wavevectors is outweighed by charge-spin coupling that locks a relatively small fraction of the available low energy fluctuations together and condenses a component of well correlated CDW order from the precursor fluctuations [50]. In view of the discontinuity in the temperature dependence (Fig. 3), it is natural to associate this behavior to the ordering of octahedral tilts that occurs at the same temperature. LTT-type octahedral tilts are known to break the 4-fold rotational symmetry of the in-plane Cu-O bonds (see the inset to Fig. 3b) generating a uni-directional field that is coupled linearly to electronic nematicity and quadratically to the CDW and SDW [24]. Such coupling generates the well correlated low temperature spin-charge locked phase that intertwines with the superconducting order parameter.

## METHODS

**Sample preparation** A $La_{1.875}Ba_{0.125}CuO_4$ single crystal was grown at Brookhaven National Laboratory using the floating zone method. The wavevectors used here are described using the high temperature tetragonal ($I4/mmm$) space group with $a = b = 3.78$ Å and $c = 13.28$ Å. The sample was cleaved ex-situ to reveal a face with a [001] surface normal and mounted with the [100] and [001] directions in the scattering plane. Correlation length are defined as 1/HWHM where HWHM is the half width at half maximum of the peak in reciprocal lattice units.

**RIXS measurements** The energy resolved resonant inelastic x-ray scattering (RIXS) measurements were performed at the ID32 beamline of the European Synchrotron Radiation Facility (ESRF, Grenoble, France) using the ERIXS spectrometer. The resonant condition was achieved by tuning the incident x-ray energy to the maximum of the Cu $L_3$ absorption peak around 931.5 eV. The scattering geometry is shown in Fig. 1a. $\sigma$ and $\pi$ x-ray polarizations are defined as perpendicular and parallel to the scattering plane, respectively. $H$ and $K$ scans are achieved by rotating the sample around the $\theta$ and $\chi$ axes, without changing $2\theta$, thus changing the in-plane component of the momentum transfer $\boldsymbol{Q} = \boldsymbol{k}_f$-$\boldsymbol{k}_i$. By doing this, we are assuming that the scattering is independent of $L$, which is reasonable as the inter-layer coupling in the cuprates is known to be weak [18, 40]. Positive (negative) $H$ corresponding to larger (smaller) $\theta$ values. The horizontal and vertical momentum resolution was 0.008 $Å^{-1}$ and 0.001 $Å^{-1}$, respectively and all intensities are normalized to beam current and counting time. Two different geometries are used here to provide sensitivity to charge and spin degrees of freedom respectively [6, 21]. For the charge scattering we used $\sigma$-polarized incident x-rays and negative $H$ values. The spectrometer scattering angle ($2\theta$) was fixed at 118° such that $L \approx 1.5$ and the total instrumental energy resolution (full-width at half maximum) was set to 90 meV to increase the counting rate. The quasi-elastic intensity was obtained by integrating the RIXS spectrum in an energy window of ± 150 meV around 0 meV. To measure the spin excitation spectra, we used $\pi$-polarized incident x-rays and positive $H$ values. The scattering angle ($2\theta$) was set at the maximum value of 149° to access higher $H$ values and the total instrumental energy resolution was set to 70 meV. The elastic energy was determined by measuring the diffuse scattering from carbon tape for every spectrum obtained.

**Calculations of the spin excitation spectrum in the CDW state** We constructed our model starting with an initial ordered set of charge stripes on a $40 \times 40$ site lattice. Stripes were spaced by 4 lattice units in order to reproduce the observed wavevector and we assume that the stripes have a width of two lattice units where the hole concentration is higher. Note that had we assumed a stripe with a width of one lattice unit, this would predict appreciable $2\boldsymbol{Q}_{\mathrm{CDW}}$ satellite peak intensity that we do not observe here. We then used a Monte Carlo algorithm to disorder the stripes until the charge structure factor matches the measured CDW peak shape. We impose constrains to forbid energetically unfavorable configurations such that stripes cannot overlap and stripes may meander, but not break completely (i.e. stripes may only deform by one lattice unit transverse to their direction at each point along their length). Having constructed a lattice with an appropriate charge configuration, we compute the magnetic excitation spectrum using a suitably parametrized Heisenberg model, with nearest neighbor magnetic exchange interaction $J$, in a very similar way to that done previously [42, 44, 45]. It is assumed that the charge stripes define domain walls across which $J$ is replaced by a ferromagnetic exchange $J_F$. In the case of a meandering stripe we insert an additional $J_F$ parallel to the stripe direction, in order to maintain well defined, unfrustrated domain walls in the colinear AF order (see Supplementary Fig. 9). We constrain $J = 165$ meV to match the observed zone boundary magnon energy observed here and $J_F = -0.09J$ was chosen to obtain the correct energy for the neck of the hourglass as observed by neutrons [51]. The magnetic excitation spectrum of the system with the domain walls is computed under the SWT approximation. This procedure is repeated to average over ten different realizations and two possible orientations of the stripes. As detailed in the main text, such a treatment is sufficient to reproduce the observed magnetic peak dispersion even without including other effects such as fermionic excitations [24, 37].

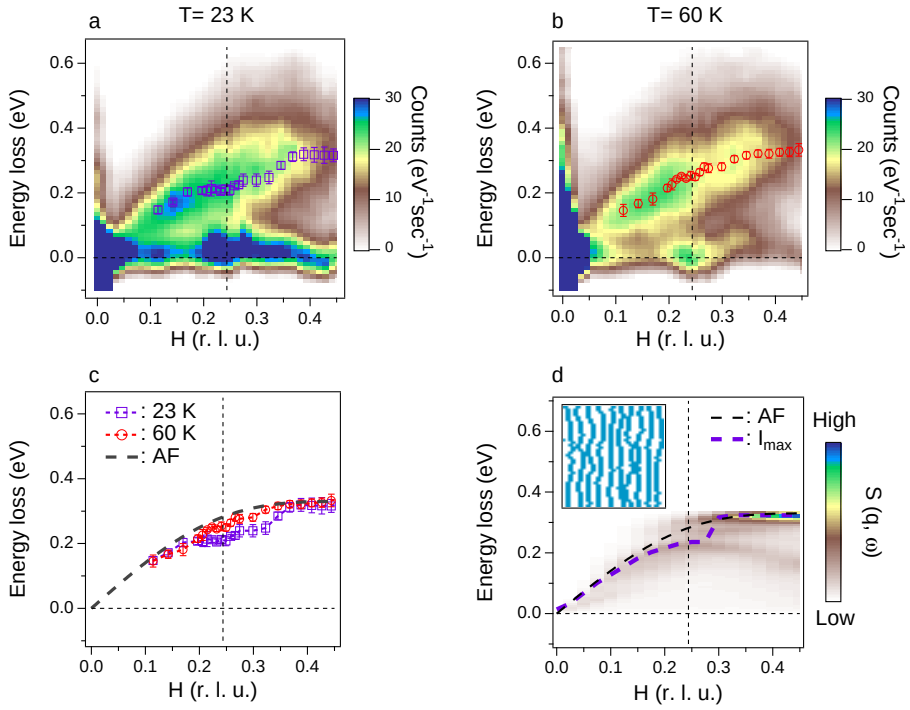


Figure 4. **Magnetic excitation spectrum and charge-spin coupling. a**,**b** RIXS intensity maps measured in a geometry that couples to the paramagnon excitation at 23 K in the low temperature CDW phase and at 60 K in the precursor CDW phase. Purple squares and red circles are the extracted peak positions from fitting the paramagnon lineshape (see Supplementary Fig. 7). **c** Comparison of the peak positions obtained by fitting the data in **a** and **b** to the dispersion expected from spin wave theory (SWT) in an antiferromagnet (AF) without stripes. **d** The inset shows the theoretical charge configuration for one realization of the meandering stripes which mimics the experimental charge structure factor at 23 K. Stripes with a width of two sites with increased hole concentration are shown in blue. The main panel shows an average of the magnetic dynamic structure factor for ten such configurations as described in the method section. The purple dashed curve connects the points of maximum intensity at each $H$ value. Such a picture qualitatively captures the observed dispersion in **c**.


## ACKNOWLEDGEMENTS

We thank Emil Bozin, Steve Kivelson, Claudio Mazzoli, T. Maurice Rice, John Tranquada and Stuart Wilkins for insightful discussions and Johnny Pelliciari for experimental assistance. RIXS research by H.M. and M.P.M.D. is supported by the Center for Emergent Superconductivity, an Energy Frontier Research Center funded by the US Department of Energy (DOE), Office of Basic Energy Sciences. Sample synthesis by G.D.G. is supported by US DOE under Contract No. DE-SC0012704. Theoretical work by J.L. is supported by the Italian MIUR under project PRIN-RIDEIRON-2012X3YFZ2. The experiment was performed using the ERIXS instrument at ID32 at the European Synchrotron Radiation Facility.


## AUTHOR CONTRIBUTIONS

Experiment: H.M., Y.Y.P., A.A., F.Y.-H., K.K., N.B.B., L.B., G.G. and M.P.M.D. Theoretical calculations: G.S. and J.L. Data analysis and interpretation: H.M., J.L., G.S., R.M.K. G.G., L.B. and M.P.M.D. Sample growth and preparation: H.M., V.T. and G.D.G. Project planning: H.M., G.G., L.B. and M.P.M.D. Paper writing: H.M. J.L., G.S., G.G., L.B. and M.P.M.D.


* hmiao@bnl.gov
† mdean@bnl.gov



[1] Zaanen, J. & Gunnarsson, O. Charged magnetic domain lines and the magnetism of high-$T_c$ oxides. *Phys. Rev. B* **40**, 7391–7394 (1989).

[2] Emery, V. J., Kivelson, S. A. & Lin, H. Q. Phase separation in the $t$ - $J$ model. *Phys. Rev. Lett.* **64**, 475–478 (1990).

[3] Castellani, C., Di Castro, C. & Grilli, M. Singular quasiparticle scattering in the proximity of charge instabilities. *Phys. Rev. Lett.* **75**, 4650–4653 (1995).

[4] Tranquada, J., Sternlieb, B., Axe, J., Nakamura, Y. & Uchida, S. Evidence for stripe correlations of spins and holes in copper oxide superconductors. *Nature* **375**, 561–563 (1995).

[5] Fujita, M., Goka, H., Yamada, K., Tranquada, J. M. & Regnault, L. P. Stripe order, depinning, and fluctuations

in $La_{1.875}Ba_{0.125}CuO_4$ and $La_{1.875}Ba_{0.075}Sr_{0.050}CuO_4$. *Phys. Rev. B* **70**, 104517 (2004).

[6] Ghiringhelli, G. *et al.* Long-Range Incommensurate Charge Fluctuations in (Y,Nd)$Ba_2Cu_3O_{6+x}$. *Science* **337**, 821–825 (2012).

[7] Chang, J. *et al.* Direct observation of competition between superconductivity and charge density wave order in $YBa_2Cu_3O_{6.67}$. *Nature Physics* **8**, 871–876 (2012).

[8] Achkar, A. J. *et al.* Distinct charge orders in the planes and chains of ortho-iii-ordered $YBa_2Cu_3\mathbf{O}_{6+\delta}$ superconductors identified by resonant elastic x-ray scattering. *Phys. Rev. Lett.* **109**, 167001 (2012).

[9] Comin, R. *et al.* Charge Order Driven by Fermi-Arc Instability in $Bi_2Sr_{2x}La_xCuO_{6+\delta}$. *Science* **343**, 390–392 (2014).

[10] da Silva Neto, E. H. *et al.* Ubiquitous interplay between charge ordering and high-temperature superconductivity in cuprates. *Science* **343**, 393–396 (2014).

[11] Thampy, V. *et al.* Rotated stripe order and its competition with superconductivity in $La_{1.88}Sr_{0.12}CuO_4$. *Phys. Rev. B* **90**, 100510 (2014).

[12] Hashimoto, M. *et al.* Direct observation of bulk charge modulations in optimally doped $Bi_{1.5}Pb_{0.6}Sr_{1.54}CaCu_2O_{8+\delta}$. *Phys. Rev. B* **89**, 220511 (2014).

[13] Tabis, W. *et al.* Charge order and its connection with Fermi-liquid charge transport in a pristine high-$T_c$ cuprate. *Nat Commun* **5**, 5875 (2014).

[14] Le Tacon, M. *et al.* Inelastic X-ray scattering in YBa2Cu3O6.6 reveals giant phonon anomalies and elastic central peak due to charge-density-wave formation. *Nat Phys* **10**, 52–58 (2014).

[15] Wang, Y. & Chubukov, A. Charge-density-wave order with momentum $(2q, 0)$ and $(0, 2q)$ within the spin-fermion model: Continuous and discrete symmetry breaking, preemptive composite order, and relation to pseudogap in hole-doped cuprates. *Phys. Rev. B* **90**, 035149 (2014).

[16] Comin, R. & Damascelli, A. Resonant X-Ray Scattering Studies of Charge Order in Cuprates. *Annual Review of Condensed Matter Physics* **7**, 369–405 (2016).

[17] Liu, Y.-H., Konik, R. M., Rice, T. & Zhang, F.-C. Giant phonon anomaly associated with superconducting fluctuations in the pseudogap phase of cuprates. *Nature communications* **7** (2016).

[18] Wilkins, S. B. *et al.* Comparison of stripe modulations in $La_{1.875}Ba_{0.125}CuO_4$ and $La_{1.48}Nd_{0.4}Sr_{0.12}CuO_4$. *Phys. Rev. B* **84**, 195101 (2011).

[19] Chen, X. M. *et al.* Remarkable stability of charge density wave order in $La_{1.875}Ba_{0.125}CuO_4$. *Phys. Rev. Lett.* **117**, 167001 (2016).

[20] Achkar, A. J. *et al.* Nematicity in stripe ordered cuprates probed via resonant x-ray scattering. *Science* **351**, 1–5 (2016).

[21] Ament, L. J. P., van Veenendaal, M., Devereaux, T. P., Hill, J. P. & van den Brink, J. Resonant inelastic x-ray scattering studies of elementary excitations. *Rev. Mod. Phys.* **83**, 705–767 (2011).

[22] Dean, M. P. M. Insights into the high temperature superconducting cuprates from resonant inelastic x-ray scattering. *Journal of Magnetism and Magnetic Materials* **376**, 3 – 13 (2015).

[23] Kivelson, S. A. *et al.* How to detect fluctuating stripes in the high-temperature superconductors. *Rev. Mod. Phys.* **75**, 1201–1241 (2003).

[24] Vojta, M. Lattice symmetry breaking in cuprate superconductors: stripes, nematics, and superconductivity. *Advances in Physics* **58**, 699–820 (2009).

[25] Nie, L., Tarjus, G. & Kivelson, S. A. Quenched disorder and vestigial nematicity in the pseudogap regime of the cuprates. *Proceedings of the National Academy of Sciences* **111**, 7980–7985 (2014).

[26] Capati, M. *et al.* Electronic polymers and soft-matter-like broken symmetries in underdoped cuprates. *Nature communications* **6** (2015).

[27] Li, Q., Hücker, M., Gu, G. D., Tsvelik, A. M. & Tranquada, J. M. Two-Dimensional Superconducting Fluctuations in Stripe-Ordered $La_{1.875}Ba_{0.125}CuO_4$. *Phys. Rev. Lett.* **99**, 067001 (2007).

[28] Bozin, E. S. *et al.* Reconciliation of local and long-range tilt correlations in underdoped $La_{2-x}Ba_xCuO_4$. *Physical Review B* **91**, 054521 (2015).

[29] Fabbris, G., Hücker, M., Gu, G. D., Tranquada, J. M. & Haskel, D. Local structure, stripe pinning, and superconductivity in $la_{1.875}ba_{0.125}cuo_4$ at high pressure. *Phys. Rev. B* **88**, 060507 (2013).

[30] Hoffman, J. *et al.* A four unit cell periodic pattern of quasi-particle states surrounding vortex cores in bi2sr2cacu2o8+ $\delta$. *Science* **295**, 466–469 (2002).

[31] Parker, C. V. *et al.* Fluctuating stripes at the onset of the pseudogap in the high-Tc superconductor Bi2Sr2CaCu2O8+x. *Nature* **468**, 677–680 (2010).

[32] Hücker, M. *et al.* Stripe order in superconducting $La_{2-x}Ba_xCuO_4$ ($0.095 \leqslant x \leqslant 0.155$). *Phys. Rev. B* **83**, 104506 (2011).

[33] Cheong, S.-W. *et al.* Incommensurate magnetic fluctuations in $La_{2-x}Sr_xCuO_4$. *Phys. Rev. Lett.* **67**, 1791–1794 (1991).

[34] Thurston, T. R. *et al.* Low-energy incommensurate spin excitations in superconducting $La_{1.85}Sr_{0.15}CuO_4$. *Phys. Rev. B* **46**, 9128–9131 (1992).

[35] Hinkov, V. *et al.* Spin dynamics in the pseudogap state of a high-temperature superconductor. *Nat Phys* **3**, 780–785 (2007).

[36] Tranquada, J. M. *et al.* Quantum magnetic excitations from stripes in copper oxide superconductors. *Nature* **429**, 534–538 (2004).

[37] Seibold, G. & Lorenzana, J. Doping dependence of spin excitations in the stripe phase of high-$T_c$ superconductors. *Phys. Rev. B* **73**, 144515 (2006).

[38] Le Tacon, M. *et al.* Intense paramagnon excitations in a large family of high-temperature superconductors. *Nat. Phys.* **7**, 725–730 (2011).

[39] Dean, M. P. M. *et al.* Spin excitations in a single $La_2CuO_4$ layer. *Nat. Mater.* **11**, 850–854 (2012).

[40] Dean, M. P. M. *et al.* Persistence of magnetic excitations in $La_{2-x}Sr_xCuO_4$ from the undoped insulator to the heavily overdoped non-superconducting metal. *Nature Materials* **12**, 1018–1022 (2013).

[41] Dean, M. P. M. *et al.* High-energy magnetic excitations in the cuprate superconductor $Bi_2Sr_2CaCu_2O_{8+\delta}$: Towards a unified description of its electronic and magnetic degrees of freedom. *Phys. Rev. Lett.* **110**, 147001 (2013).

[42] Carlson, E. W., Yao, D. X. & Campbell, D. K. Spin waves in striped phases. *Phys. Rev. B* **70**, 064505 (2004).

[43] Seibold, G. & Lorenzana, J. Magnetic fluctuations of stripes in the high temperature cuprate superconductors. *Phys. Rev. Lett.* **94**, 107006 (2005).

[44] Yao, D. X., Carlson, E. W. & Campbell, D. K. Magnetic excitations of stripes and checkerboards in the cuprates. *Phys. Rev. B* **73**, 224525 (2006).

[45] Yao, D. X., Carlson, E. W. & Campbell, D. K. Magnetic excitations of stripes near a quantum critical point. *Phys. Rev. Lett.* **97**, 017003 (2006).

[46] Lorenzana, J. & Seibold, G. Metallic mean-field stripes, incommensurability, and chemicalpotential in cuprates. *Phys. Rev. Lett.* **89**, 136401 (2002).

[47] Seibold, G., Grilli, M. & Lorenzana, J. Stripes in cuprate superconductors: Excitations and dynamic dichotomy. *Physica C: Superconductivity* **481**, 132–145 (2012).

[48] Valla, T., Fedorov, A. V., Lee, J., Davis, J. C. & Gu, G. D. The Ground State of the Pseudogap in Cuprate Superconductors. *Science* **314**, 1914–1916 (2006).

[49] Zachar, O. Stripes disorder and correlation lengths in doped antiferromagnets. *Phys. Rev. B* **62**, 13836–13839 (2000).

[50] Zachar, O., Kivelson, S. A. & Emery, V. J. Landau theory of stripe phases in cuprates and nickelates. *Phys. Rev. B* **57**, 1422–1426 (1998).

[51] Tranquada, J. M. *et al.* Evidence for unusual superconducting correlations coexisting with stripe order in $La_{1.875}Ba_{0.125}CuO_4$. *Phys. Rev. B* **78**, 174529 (2008).